PROCEEDINGS OF SCIENCE

Kilonova emission from realistic neutron star merger simulations

Christine E. Collins,[a,*] **Andreas Bauswein,**[a] **Stuart A. Sim,**[b] **Vimal Vijayan,**[a,c] **Gabriel Martínez-Pinedo,**[a,d] **Oliver Just,**[a,e] **Luke J. Shingles**[a] **and Markus Kromer**[f]

[a] *GSI Helmholtzzentrum für Schwerionenforschung, Planckstraße 1, 64291 Darmstadt, Germany*

[b] *Astrophysics Research Center, School of Mathematics and Physics, Queen's University Belfast, Belfast BT7 1NN, Northern Ireland, UK*

[c] *Department of Physics and Astronomy, Ruprecht-Karls-Universität Heidelberg, Im Neuenheimer feld 226, 69120 Heidelberg, Germany*

[d] *Institut für Kernphysik (Theoriezentrum), Fachbereich Physik, Technische Universität Darmstadt, Schlossgartenstraße 2, 64289 Darmstadt, Germany*

[e] *Astrophysical Big Bang Laboratory, RIKEN Cluster for Pioneering Research, 2-1 Hirosawa, Wako, Saitama 351-0198, Japan*

[f] *Heidelberger Institut für Theoretische Studien (HITS), Schloss-Wolfsbrunnenweg 35, 69118 Heidelberg*

E-mail: c.collins@gsi.de

The detection of GW170817 and its electromagnetic counterpart AT2017gfo confirmed the expectation that a kilonova would accompany the merging of binary neutron stars, and subsequently there has been much interest in simulating kilonova emission to better understand the observations of AT2017gfo. The majority of models considered when predicting kilonova emission have been 1D, or even idealised toy models. Few simulations have been based on realistic merger simulations, and fewer have carried out full 3D simulations of the merger and subsequent kilonova emission. We present 3D radiative transfer simulations based on the dynamical ejecta from 3D smoothed-particle hydrodynamics neutron star merger simulations, including a sophisticated neutrino treatment. Nucleosynthesis calculations following the SPH trajectories provide the energy released due to radioactive decays of r-process material. We discuss the predicted light curves in different lines of sight, as well as the influence of the assumptions we make on the light curve evolution. This includes our assumption of opacities based on the electron fraction of the material, which is predominantly responsible for the distribution of r-process elements synthesised. We find that the light curves show a modest viewing angle dependence.

FAIR next generation scientists - 7th Edition Workshop
23-27 May 2022
Paralia, Greece

*Speaker

PoS(FAIRness2022)010

1. Introduction

A kilonova is the electromagnetic counterpart accompanying the merging of binary neutron stars. This has recently been unambiguously observed for the first time, where AT2017gfo [25,29] was coincident with the gravitational wave signal GW170817 [1] which was consistent with a binary neutron star merger. When binary neutron stars merge, the neutron rich environment allows r-process nucleosynthesis to take place. The radioactive decays of freshly synthesised r-process elements power an optical kilonova transient. To better understand kilonovae, we require detailed binary neutron star merger simulations, and self-consistent radiative transfer calculations to compare simulations directly to observations. Binary neutron star mergers show strong asymmetries in the ejecta [5], necessitating multi-dimensional radiative transfer simulations to produce line of sight dependent synthetic observables. Many previous works have carried out radiative transfer simulations based on analytical models described by simplified physics (e.g. power-law density structures or idealised geometries) [3,7–9,16,18,22,30,32]. Of the radiative transfer simulations considering real merger simulations, most have been carried out in 2D [12–15], with only a few in 3D [19,27]. Here we present a 3D radiative transfer simulation based on a 3D binary neutron star merger simulation. We compare the viewing-angle dependent light curves to observations of AT2017gfo (see Collins et al. [6] for further details).

2. Overview of simulations

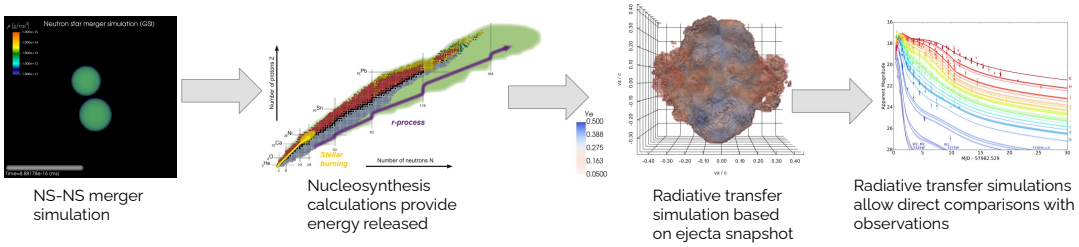

Figure 1: Self-consistent modelling pipeline for comparing kilonova simulations to observations. A binary neutron star merger simulation is carried out (image from S. Blacker), followed by detailed nuclear network calculations for each SPH particle trajectory (image credit: EMMI, GSI/Different Arts). Radiative transfer calculations are carried out using a snapshot of the simulated ejecta, which can be directly compared to observations (shown are the light curves of AT2017gfo by Villar et al. [29]).

The aim of this research is to predict synthetic observables for a realistic neutron star merger simulation. We use the 3D Monte Carlo radiative transfer code ARTIS [17,23,24] to predict angle dependent light curves. We consider a merger simulation of equal mass binary neutron stars (BNS), each 1.35 $M_\odot$, which is simulated by a 3D general relativistic smoothed-particle hydrodynamics (SPH) code, that includes an advanced neutrino treatment (ILEAS [2]). We use a self-consistent modelling pipeline to directly compare simulations to observations (see Fig. 1). After the BNS merger simulation, nuclear network calculations are carried out for each of the SPH particle trajectories that were gravitationally unbound. A snapshot of merger ejecta is taken (and mapped to a Cartesian grid) as the input to the radiative transfer calculation, and the energy powering the kilonova is taken from the nuclear network calculations. The radiative transfer simulation produces light curves, which can be directly compared to observations.

The BNS merger simulation predicts highly asymmetric ejecta, where the polar directions have much lower densities than equatorial lines of sight. Here we only consider dynamical ejecta, expelled on timescales of milliseconds after the merger (20 milliseconds after both stars touched). The total mass of the dynamical ejecta mapped onto the radiative transfer simulation grid is 0.0051 $M_\odot$. We assume a grey approximation in the radiative transfer[24] and assume grey absorption cross sections based on the electron fraction (Y_e) of the ejecta (see Table 1). A low Y_e produces a high lanthanide fraction, and therefore high opacities while a high Y_e produces a low lanthanide fraction and lower opacities. In our model, the polar directions show a higher Y_e than the equatorial directions.

Table 1: Mass absorption cross sections (κ) adopted in this study for each electron fraction Y_e range[28]. *The lowest Y_e opacity is underestimated due to lack of complete atomic data for actinides[28].

Y_e	κ cm^2 g^{-1}
$Y_e \leq 0.1$	19.5*
$0.1 < Y_e \leq 0.15$	32.2
$0.15 < Y_e \leq 0.2$	22.3
$0.2 < Y_e \leq 0.25$	5.60
$0.25 < Y_e \leq 0.3$	5.36
$0.3 < Y_e \leq 0.35$	3.30
$Y_e > 0.35$	0.96

The kilonova is powered by radioactive β-decays, α-decays and fission. The nuclear network calculations show that most of the heating in this model takes the form of β-decays, and therefore we assume that all heating in our simulation is from β-decays. The emitted neutrinos are not expected to thermalise, and we assume 35% of the total energy is lost to neutrinos. We assume γ-rays account for 45% of the β-decay energy, and β-particles account for 20% of the energy[4]. We include a γ-ray transport scheme for estimated γ-ray energies[4], and assume β-particles thermalise instantaneously. The total energy in each model grid cell is determined from the SPH particle trajectories (allowing for a spatially dependent energy distribution), but we assume the same rate of energy generation for the entire ejecta, given as the average energy generation rate of all SPH trajectories.

3. Results

The angle-dependent light curves calculated from our radiative transfer simulation are shown in Fig. 2. Lines of sight in the polar directions are brighter than equatorial directions, due to lower grey opacities and lower densities. The bolometric (Ultraviolet-Infrared) light curves do not rise to a peak, but instead a 'shoulder' is seen as the bulk ejecta become optically thin. Energy is generated and thermalised in high velocity, outer regions of the ejecta, where the optical depths are low, and therefore radiation is able to escape the ejecta from very early times, leading to the monotonic decline of the bolometric light curves.

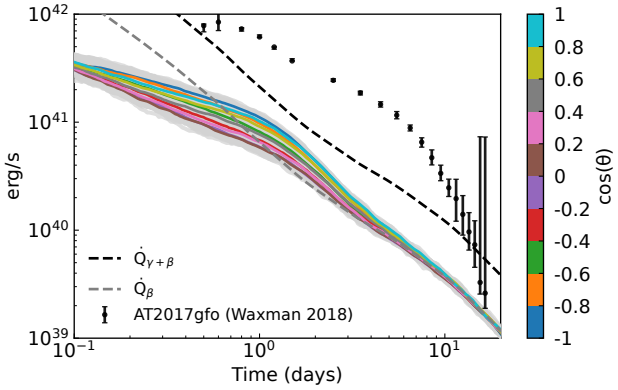

Figure 2: Line of sight bolometric UVOIR light curves. Each coloured line is the azimuthally averaged light curve (averaged over each angle bin in cos(θ)), while all 100 uniformly spaced viewing angle bins are plotted in light grey. Also marked is the total energy released (on average) by nuclear reactions, $\dot{Q}_{\gamma+\beta}$ (excluding energy assumed to be lost to neutrinos), and the energy due to β-particles ($\dot{Q}_\beta$). The bolometric light curve of AT2017gfo[31] is plotted for reference.

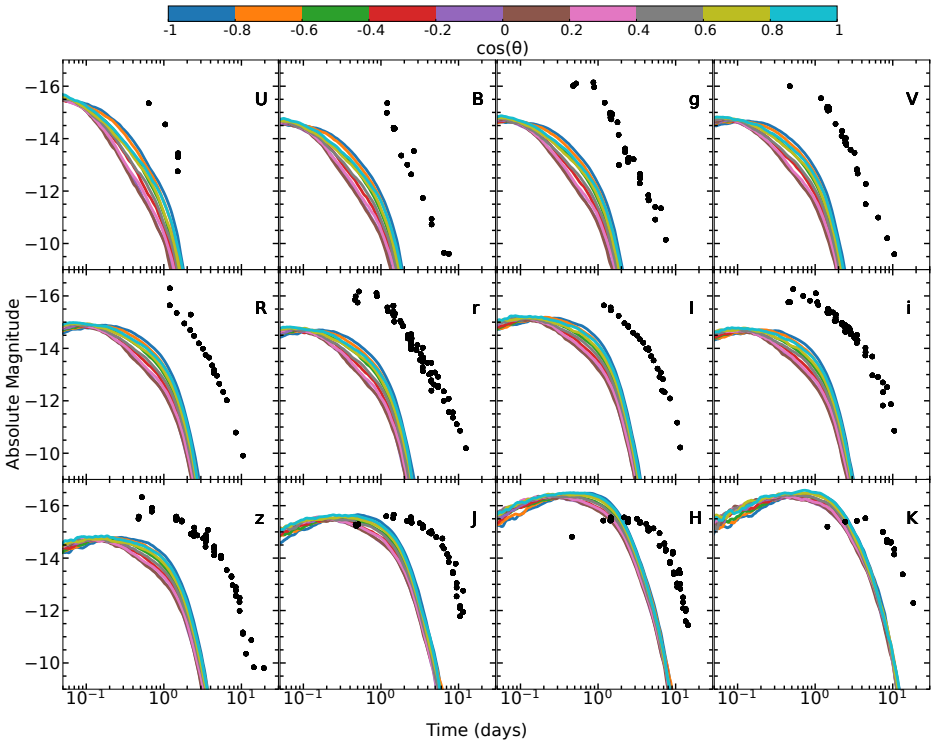

Figure 3: Light curves estimated from radiation temperature. Also plotted are the light curves for AT2017gfo[29], assuming a distance of 40 Mpc.

The mass of the dynamical ejecta we consider here are less massive than the mass that was inferred for AT2017gfo[25], and therefore less energy is generated and the light curve of our model is not as bright. The total energy available for heating the ejecta is marked on Fig. 2 (γ-ray and β-particle energy, neutrino energy is already excluded from this). Also marked is the energy available from β-particles. The late time light curve is dependent on the rate of energy thermalising, and in our model after ~5 days this is entirely dependent on the β-particle rate. For the late time light curve, accurately calculating the amount of energy from β-particles will be important and should be investigated in future. We find that γ-rays only thermalise at very early times (< 2 hours). After this time the γ-ray light curve is determined solely by the total γ-ray energy. No viewing angle dependence is expected in the γ-light curve.

3.1 Approximate spectral-band light curves

We do not calculate any frequency dependence in our simulation, and therefore we can not directly extract spectral band limited light curves from the simulation. However, we estimate frequencies from the radiation temperature at the location where radiation was emitted. Specifically, we randomly sample a frequency from a black body distribution peaking at the radiation temperature. From this we obtain approximate spectral band-light curves, which are plotted in Fig. 3. Due to the temperature evolution alone, we find a similar light curve evolution to that shown by AT2017gfo[29], although on shorter timescales. We also find that the light curves show a rapid blue to red colour evolution, similar to that shown by AT2017gfo (see Fig. 4).

3.2 Secular ejecta

In addition to the dynamical ejecta simulation, we carried out a simulation for a model with combined dynamical ejecta (as above) and secular ejecta components. Mass from the torus and wind components of a long term evolution simulation (similar to Just et al. [11], see Collins et al. [6]), which we angle-averaged, was added to the mass distribution of the dynamical ejecta model. The extra mass is 0.019 $M_\odot$, giving a total ejecta mass of 0.024 $M_\odot$. The additional mass at the centre of the ejecta (at low velocities) leads to increased energy deposition in the central regions of the ejecta. This energy begins to escape the ejecta around 1 day, visible in the light curve as the increased brightness of the 'shoulder'. The early light curve shows little change due to the secular ejecta component. This suggests that to match the brightness of the early time light curve observed for AT2017gfo more mass is required at high velocities than in our dynamical ejecta model.

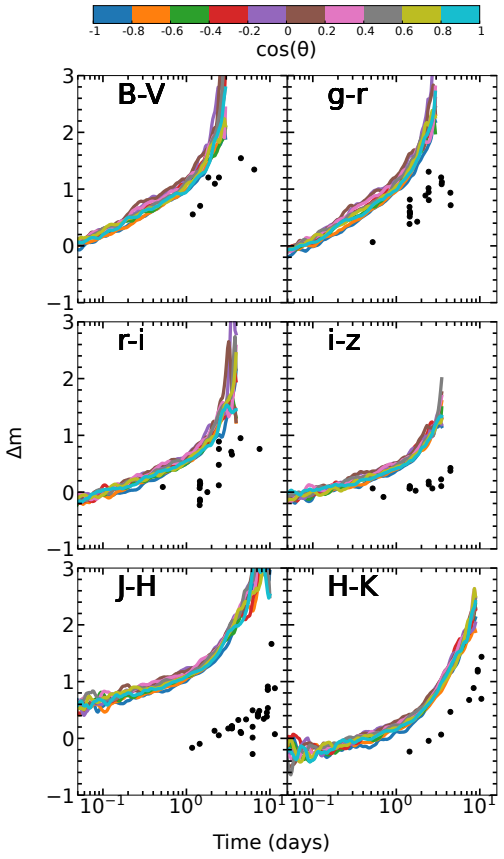

Figure 4: Angle-averaged colour evolution, estimated from radiation temperature. Also plotted are the colours of AT2017gfo[29].

4. Conclusions

We presented viewing-angle dependent bolometric light curves, based on realistic binary neutron star merger simulations. The light curves in the polar directions are up to a factor of ~2 brighter than equatorial lines of sight. The bolometric light curves do not rise to a peak, but show a 'shoulder' at the time where the bulk ejecta become optically thin.

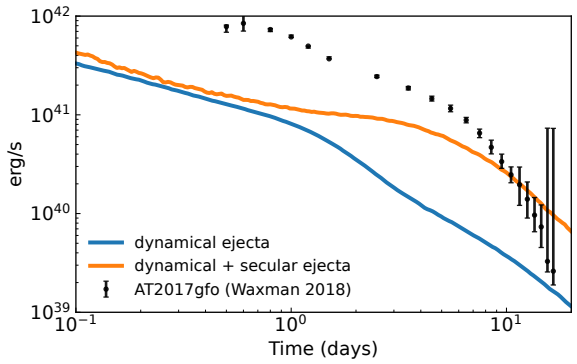

Figure 5: Bolometric angle-averaged light curves for the model including the secular ejecta component and without. Also plotted is the bolometric light curve of AT2017gfo[31].

In future, determining the exact energy fractions going into β-particles, γ-rays and neutrinos will be important, particularly for the late time light curve, since after ~5 days the light curve is dependent on the total energy that thermalised in the ejecta. Due to the temperature evolution, we found a rapid colour evolution from blue to red, similar to that observed in AT2017gfo. This suggests that the colour evolution could be driven by cooling, rather than the elemental composition of the ejecta. Additional mass is required at high velocities to match the observed brightness of AT2017gfo, as the early time light curve brightness is not increased by low velocity, secular ejecta.

Acknowledgements

We thank Ricard Ardevol-Pulpillo and Thomas Janka for providing the ILEAS scheme. CEC, AB and OJ acknowledge support by the European Research Council (ERC) under the European Union's Horizon 2020 research and innovation program under grant agreement No. 759253. AB, G.M.-P and OJ acknowledge support by Deutsche Forschungsgemeinschaft (DFG, German Research Foundation) - Project-ID 279384907 - SFB 1245. AB and VV acknowledge support by DFG - Project-ID 138713538 - SFB 881 ("The Milky Way System", subproject A10). AB and G.M.-P acknowledge support by the State of Hesse within the Cluster Project ELEMENTS. The work of SAS was supported by the Science and Technology Facilities Council [grant numbers ST/P000312/1, ST/T000198/1]. G.M.-P and LJS acknowledge support by the European Research Council (ERC) under the European Union's Horizon 2020 research and innovation program (ERC Advanced Grant KILONOVA No. 885281). This work was performed using the Cambridge Service for Data Driven Discovery (CSD3), part of which is operated by the University of Cambridge Research Computing on behalf of the STFC DiRAC HPC Facility (www.dirac.ac.uk). The DiRAC component of CSD3 was funded by BEIS capital funding via STFC capital grants ST/P002307/1 and ST/R002452/1 and STFC operations grant ST/R00689X/1. DiRAC is part of the National e-Infrastructure. OJ is grateful for computational support by the HOKUSAI computing facility at RIKEN. CEC, OJ and VV are grateful for computational support by the VIRGO cluster at GSI. NumPy and SciPy[20], IPython[21], Matplotlib[10], PyVista[26] and ARTISTOOLS[1] were used for data processing and plotting.

References

1. Abbott B. P., et al., 2017, Phys. Rev. Lett., 119, 161101
2. Ardevol-Pulpillo R., Janka H. T., Just O., Bauswein A., 2019, MNRAS , 485, 4754
3. Banerjee S., Tanaka M., Kawaguchi K., Kato D., Gaigalas G., 2020, ApJ, 901, 29
4. Barnes J., Kasen D., Wu M.-R., Martínez-Pinedo G., 2016, ApJ, 829, 110
5. Bauswein A., Goriely S., Janka H.-T., 2013, ApJ, 773, 78
6. Collins C. E., Bauswein A., Sim S. A., Vijayan V., Martínez-Pinedo G., Just O., Shingles L. J., Kromer M., 2023, MNRAS , 521, 1858
7. Domoto N., Tanaka M., Wanajo S., Kawaguchi K., 2021, ApJ, 913, 26
8. Even W., et al., 2020, ApJ, 899, 24
9. Heinzel J., et al., 2021, MNRAS , 502, 3057
10. Hunter J. D., 2007, Computing in Science & Engineering, 9, 90
11. Just O., Bauswein A., Ardevol Pulpillo R., Goriely S., Janka H. T., 2015, MNRAS , 448, 541
12. Just O., Kullmann I., Goriely S., Bauswein A., Janka H. T., Collins C. E., 2022, MNRAS , 510, 2820
13. Kasen D., Fernández R., Metzger B. D., 2015, MNRAS , 450, 1777
14. Kawaguchi K., Fujibayashi S., Shibata M., Tanaka M., Wanajo S., 2021, ApJ, 913, 100
15. Kawaguchi K., Fujibayashi S., Hotokezaka K., Shibata M., Wanajo S., 2022, ApJ, 933, 22
16. Korobkin O., et al., 2021, ApJ, 910, 116
17. Kromer M., Sim S. A., 2009, MNRAS , 398, 1809
18. Metzger B. D., et al., 2010, MNRAS , 406, 2650
19. Neuweiler A., Dietrich T., Bulla M., Chaurasia S. V., Rosswog S., Ujevic M., 2023, Phys. Rev. D, 107, 023016
20. Oliphant T. E., 2007, Computing in Science & Engineering, 9, 10
21. Pérez F., Granger B. E., 2007, Computing in Science & Engineering, 9, 21
22. Pognan Q., Jerkstrand A., Grumer J., 2022, MNRAS , 510, 3806
23. Shingles L. J., et al., 2020, MNRAS , 492, 2029
24. Sim S. A., 2007, MNRAS , 375, 154
25. Smartt S. J., et al., 2017, Nature, 551, 75
26. Sullivan C. B., Kaszynski A., 2019, Journal of Open Source Software, 4, 1450
27. Tanaka M., Hotokezaka K., 2013, ApJ, 775, 113
28. Tanaka M., Kato D., Gaigalas G., Kawaguchi K., 2020, Monthly Notices of the Royal Astronomical Society, 496, 1369
29. Villar V. A., et al., 2017, ApJ, 851, L21
30. Watson D., et al., 2019, Nature, 574, 497

[1] https://github.com/artis-mcrt/artistools/

31. Waxman E., Ofek E. O., Kushnir D., Gal-Yam A., 2018, MNRAS , 481, 3423
32. Wollaeger R. T., et al., 2021, ApJ, 918, 10